Article

946/1030 nm Dual-Wavelength Laguerre-Gaussian (LG$_{01}$) Mode Vortex Laser Based on Intracavity Cascade Pumped Resonator

Yashuai Yang, Yongliang Li *, Chi Wang and Chao Yang

School of Opto-Electronics Engineering, Changchun University of Science and Technology,
Changchun 130022, China; yangyashuai@mails.cust.edu.cn (Y.Y.); wangchi@mails.cust.edu.cn (C.W.);
yangchao@cust.edu.cn (C.Y.)
* Correspondence: liyongliang@cust.edu.cn

Abstract: In this paper, the 946/1030 nm dual-wavelength LG$_{01}$ mode vortex laser is obtained by applying the intracavity cascade pumped structure and annular-beam end-pumped method, an innovative and pioneering exploration of the transverse mode of the dual-wavelength laser. First, we demonstrate the oscillation characteristic theoretical model of the dual-wavelength LG$_{01}$ mode laser, considering the reabsorption effect. Then the length of the laser crystal and the transmittance of the output mirror are simulated and analyzed, respectively, related to the oscillation characteristics of the 946 and 1030 nm LG$_{01}$ mode vortex lasers. Finally, a 946/1030 nm LG$_{01}$ mode vortex laser with the same handedness is successfully achieved in our experiment. With 20 W of annular-beam pump power, the output power of 946 and 1030 nm LG$_{01}$ mode vortex lasers is 0.404 and 0.510 W, the slope efficiency is 3.6% and 6.2%, and the total optical-optical conversion efficiency is 4.6%. At the maximum output power, the fluctuations of output power within 1 h are 4.02% and 4.23%, and the beam quality factors M^2 are 2.32 and 2.27, respectively, for 946 and 1030 nm LG$_{01}$ mode vortex lasers. The wavefront phase $\exp(i\phi)$ of the 946/1030 nm dual-wavelength is also proved by the self-interference method.

Keywords: dual-wavelength laser; LG$_{01}$ mode; intracavity pumped

1. Introduction

A dual or multi-wavelength laser can output two or more different laser wavelengths in a single device. Compared with combining laser beams output from two or more independent lasers utilizing dispersion elements, dual or multi-wavelength lasers have the advantages of compactness, simplicity, and reliability. At present, dual or multi-wavelength lasers are mainly obtained in solid-state lasers by controlling the gain-loss between different wavelengths or in semiconductor and fiber lasers based on comb filters to suppress mode competition [1–3]. Because of their simple structure, diverse operation modes, and high beam quality, research on dual and multi-wavelength has long been of great significance in the field of lasers. Reviewing the development of research on dual or multi-wavelength solid-state lasers, there has been a lot of extended research on dual-wavelength lasers, such as novel wavelength combination [4–7], pulse modulation [8–10], power-ratio tuning [11–13], linewidth compression [14,15], and gain competition management [16–18], etc. However, as far as it is known, little research has been conducted on output transverse modes among the many extended studies of dual or multi-wavelength lasers.

LG mode beams have the unique properties of an annular-shaped profile, spiral wavefront, and orbital angular momentum(OAM), and they are widely used in optical tweezers [19,20], super-resolution microscopic imaging [21], quantum information processing [22], optical communications [23]. Recently, OAM beams also have found applications in a couple of new fields, such as defect detection in nanostructures [24], artificial spin ice systems [25], direction-sensitive detection of spinning objects [26], and the first reliable

ptychographic imaging of highly periodic structures [27]. In addition, dual or multi-wavelength lasers are widely used in biomedicine [28], laser detection [29], terahertz wave generation [30], nonlinear optical mixing [31], etc. Combining the concepts of vortex light and dual-wavelength, the dual-wavelength vortex laser as a new type of laser will have important potential application value in some fields mentioned above. Among them, the dual-wavelength vortex laser can play a further role in conducting intracavity sum-frequency experiments to obtain LG mode vortex laser in the blue wavelength band, which has not been reported yet; and variability of topological charge during the sum-frequency process can also be investigated.

In this paper, a 946/1030 nm dual-wavelength LG_{01} mode vortex laser is first proposed by taking the intracavity cascade pumping structure and annular-beam end-pumped method. For the Section 2, the oscillation characteristic model of a 946/1030 nm intracavity cascade pumped dual-wavelength LG_{01} mode laser is established. For the Section 3, the length of the laser crystal and the transmittance of the output mirror are under analysis, respectively, related to both the oscillation characteristics of the 946 nm (threshold pump power, output power, and intracavity power) and 1030 nm (threshold pump power and output power) LG_{01} mode vortex laser. For the Section 4, the 946 and 1030 nm dual-wavelength LG_{01} mode vortex laser with the same handedness is obtained, and the output power is 0.404 and 0.510 W at the 20 W annular-beam pump power, respectively. Details of the study of the 946/1030 nm dual-wavelength LG_{01} mode vortex laser are given in the following sections.

2. Theoretical Analysis

The energy level schematic of the intracavity cascading pumped method is shown in Figure 1. An Nd:YAG crystal is pumped by an 808 nm laser diode (LD) to achieve a 946 nm laser through energy level transition ($^4F_{3/2} \rightarrow {}^4I_{9/2}$), and then a Yb:YAG crystal is directly pumped by 946 nm in the resonant cavity to achieve a 1030 nm laser through energy level transition ($^4F_{5/2} \rightarrow {}^4I_{7/2}$). The operation schematic of the intracavity cascading pumped method is shown in Figure 2. Nd:YAG and Yb:YAG crystals are all located in the resonant cavity, and the 1030 nm resonant cavity is located in the 946 nm resonant cavity. The Nd:YAG crystal is pumped by 808 nm LD to achieve a 946 nm laser, and then the Yb:YAG crystal is directly pumped by 946 nm in the resonant cavity to realize a 1030 nm laser, finally realizing a 946/1030 nm dual-wavelength laser output. The 946 and 1030 nm lasers come from two crystals, respectively, so the intracavity cascade pumped scheme avoids the gain competition between spectral lines.
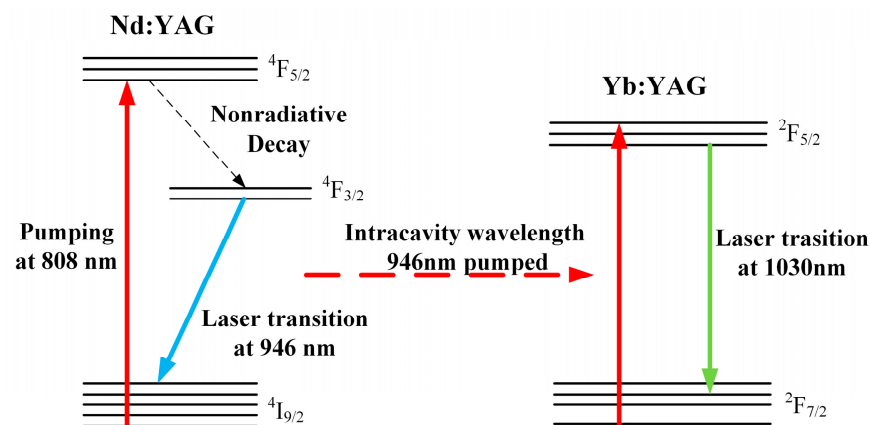

Figure 1. The energy level schematic of the intracavity cascading pumped method.
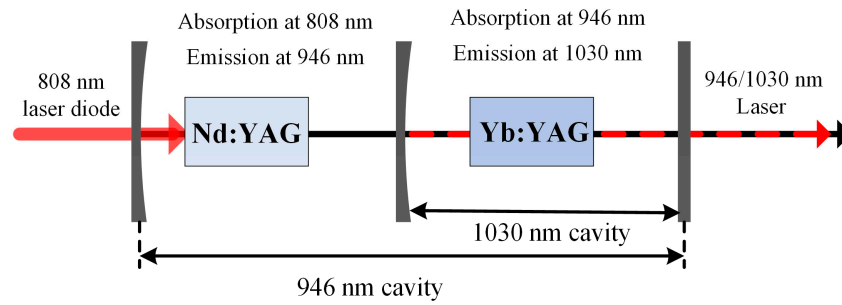
Figure 2. The operation schematic of the intracavity cascading pumped method.

In end-pumped solid-state lasers, different modes of laser can be obtained based on the pump light with different irradiance distribution or pumping off-axis gain medium, such as the TEM_{00} mode, Hermite–Gaussian (HG) mode, and LG mode. The TEM_{00} mode laser is obtained when the light source with point irradiance distribution pumps the gain medium along the direction of the optical axis, which is the pump source and pumping method used in the vast majority of lasers at present [32,33]. The HG mode laser can be excited by pumping off-axis with the help of a fiber-coupled laser diode, and the order of the HG laser will be increased as the transverse separation of the fiber from the optical axis increases [34,35]. In addition, the HG mode laser can be converted to an LG mode laser using a cylindrical lens set outside the resonant cavity, which is also an indirect method to obtain the LG mode laser [36]. However, a laser with annular-shaped irradiance distribution end-pumped gain media is currently more common for obtaining the LG laser [37,38]. Because the pump beam with an annular-shaped irradiance distribution and the LG laser has good mode-matching effects in the gain medium, the LG laser can be obtained directly in the cavity based on this method. In the previous work, we obtained a 946 nm LG_{01} mode vortex laser by end-pumped Nd:YAG crystal with an 808 nm annular beam [39]. The 946 nm LG_{01} mode vortex laser has a two-lobe transverse irradiance distribution at any position in the cavity. Meanwhile, the light irradiance of a 946 nm LG_{01} mode vortex laser within a distance is superposed in the resonator to obtain an annular distribution, which can achieve a good mode-matching effect with a 1030 nm vortex laser equipped with Yb:YAG crystal.

Next, assuming that the pump beam is of an annular-shaped irradiance distribution and the output laser is of the LG_{01} mode, the oscillatory characteristic model of the 946/1030 nm intracavity cascade pumped dual-wavelength LG_{01} mode laser considering the reabsorption effect is established. The rate equations describing the intracavity cascaded pumped dual-wavelength laser can be expressed as:

$$\frac{d\Delta N_I(r,z)}{dt} = f_I \Psi_I \xi_{pI}(r,z) - \frac{\Delta N_I(r,z) - \Delta N_I{}^0(r,z)}{\tau_I} - \frac{c}{n_I} \sigma_I f_I \Delta N_I(r,z) \Phi_I \varphi_{0I}(r) \tag{1}$$

$$\frac{d\Phi_I}{dt} = \frac{c\sigma_I}{n_I} \iiint \Delta N_I(r,z) \Phi_I \varphi_{0I}(r) dV - \frac{\Phi_I}{\tau_{qI}} \tag{2}$$

$$\frac{d\Delta N_{II}(r,z)}{dt} = f_{II} \Psi_{II} \xi_{pII}(r,z) - \frac{\Delta N_{II}(r,z) - \Delta N_{II}^0(r,z)}{\tau_{II}} - \frac{c}{n_{II}} \sigma_{II} f_{II} \Delta N_{II}(r,z) \Phi_{II} \varphi_{0II}(r) \tag{3}$$

$$\frac{d\Phi_{II}}{dt} = \frac{c\sigma_{II}}{n_{II}} \iiint \Delta N_{II}(r,z) \Phi_{II} \varphi_{0II}(r) dV - \frac{\Phi_{II}}{\tau_{qII}} \tag{4}$$

where the subscripts *I* and *II* are used to represent the parameters in the 946 and 1030 nm resonators, respectively. ΔN is the population inversion density; Φ is the photon number density in the resonant cavity; Ψ is the pumping rate; ξ_p is the photon spatial distribution function of the pump beam; ΔN^0 is the distribution function of the natural particle number inversion in the thermal equilibrium state without pumping; τ is the fluorescence lifetime

of the particles involved in the transition of the upper energy level of the laser crystal; c is the speed of light; n is the refractive index of the laser crystal; σ is the emission cross-section of the oscillating light; φ_0 is the photon spatial distribution function of the oscillating beam; τ_q is the intracavity photon lifetimes; $f = f_1 + f_2$, f_1 and f_2 are the ratio of the number of upper and lower level particles participating in the transition to the total number of lower level particles.

The 808 nm beam with an annular-shaped profile as the pump source and the 946 nm LG_{01} mode vortex laser as the intracavity pump source ξ_p can be expressed as [40]:

$$\xi_{PI}(r,z) = \begin{cases} \dfrac{\alpha_{pI}\exp(-\alpha_{pI}z)}{\pi(b^2-a^2)(1-\exp(-\alpha_{pI}d_I))} & (a \leq r \leq b) \\ 0 & elsewhere \end{cases} \tag{5}$$

$$\xi_{PII}(r,z) = \frac{4r^2}{\pi\omega_{0I}{}^4}\frac{\alpha_{pII}\exp(-\alpha_{pII}z)}{1-\exp(-\alpha_{pII}d_{II})}\exp\left(-\frac{2r^2}{\omega_{0I}{}^2}\right) \tag{6}$$

where α_p is the absorption coefficient of the laser crystal to the pump beam; d is the length of the laser crystal; b is the outer radius of the annular beam; a is the inner radius of the annular beam; ω_0 is the beam waist radius of the fundamental mode in the laser crystal.

Under stable operation, the normalized irradiance distribution function per unit volume in laser crystals φ_0 for 946 and 1030 nm LG_{01} mode vortex lasers is:

$$\varphi_{0I}(r) = \frac{4r^2}{\pi\omega_{0I}{}^4 d_I}\exp\left(-\frac{2r^2}{\omega_{0I}{}^2}\right) \tag{7}$$

$$\varphi_{0II}(r) = \frac{4r^2}{\pi\omega_{0II}{}^4 d_{II}}\exp\left(-\frac{2r^2}{\omega_{0II}{}^2}\right) \tag{8}$$

Other single-round losses L_I (except transmission loss γ_{TI} and reabsorption loss $2N_{1I}^0\sigma_I d_I$) in the 946 nm laser resonator include the loss of the resonator itself L_{0I}, the absorption loss γ_α caused by the Yb:YAG crystal, and the insertion loss R_{loss} caused by the total reflection mirror of the 1030 nm laser resonator. Other single-round losses in the 1030 nm laser resonator only are considered for the loss of the resonator itself L_{0II}. In the 946 and 1030 nm laser resonators, the smallest size elements are the Nd:YAG and Yb:YAG crystals, which are much larger than the radius of the mode. Compared to several other losses, the diffraction losses caused by the crystals can be almost negligible such that we can attribute the losses caused by them to a part of the loss term of the intracavity itself. On this basis, the expressions of the threshold pump power P_{thI}, output power P_{outI}, and intracavity power P_{inI} of the 946 nm LG_{01} mode vortex laser are established:

$$P_{thI} = \frac{\pi h v_{pI}\left(L_{0I}+\gamma_{\alpha I}+R_{loss}+\gamma_{TI}+2N_{1I}^0\sigma_I d_I\right)\left(b^2-a^2\right)}{2\sigma_I\tau_I\eta_{\alpha I}(f_{1I}+f_{2I})} \\ \left[\frac{1}{\left[\left(\frac{2a^2}{\omega_o{}_I{}^2}\right)\exp\left(-\frac{2a^2}{\omega_o{}_I{}^2}\right)-\left(\frac{2b^2}{\omega_o{}_I{}^2}\right)\exp\left(-\frac{2b^2}{\omega_o{}_I{}^2}\right)+\exp\left(-\frac{2a^2}{\omega_o{}_I{}^2}\right)-\exp\left(-\frac{2b^2}{\omega_o{}_I{}^2}\right)\right]}\right] \tag{9}$$

$$P_{outI} = \frac{2T_I\left(P_p-P_{thI}\right)\omega_{oI}{}^2\eta_{\alpha I}h v_{oI}/h v_{pI}}{(L_{0I}+\gamma_{\alpha I}+R_{loss}+\gamma_{TI})(b^2-a^2)} \tag{10}$$

$$P_{inI} = \frac{1+R_I}{1-R_I}\frac{2T_I\left(P_p-P_{thI}\right)\omega_{oI}{}^2\eta_{\alpha I}h v_{oI}/h v_{pI}}{(L_{0I}+\gamma_{\alpha I}+R_{loss}+\gamma_{TI})(b^2-a^2)} \tag{11}$$

The intracavity power of the 946 nm LG_{01} mode laser is used as the pump power of the 1030 nm LG_{01} mode laser. Further, the output power $P_{out\Pi}$ and threshold pump power $P_{th\Pi}$ of the 1030 nm LG_{01} mode vortex laser is expressed as:

$$P_{out\Pi} = \frac{4T_\Pi(P_{inI} - P_{th\Pi})\eta_{\alpha\Pi}h\nu_{o\Pi}/h\nu_{oI}}{6\left(L_{o\Pi} + \gamma_{T\Pi} + 2N_{1\Pi}^0\sigma_\Pi d_\Pi\right)\frac{C_1}{C_2} - N_{1\Pi}^0\sigma_\Pi d_\Pi C_3} \tag{12}$$

$$P_{th\Pi} = \frac{\pi h\nu_{p\Pi}\left(L_{0\Pi} + \gamma_{T\Pi} + 2N_{1\Pi}^0\sigma_\Pi d_\Pi\right)\left(\frac{\omega_{0\Pi}^4}{\omega_{0I}^2} + 3\omega_{0I}^2 + 3\omega_{0\Pi}^2 + \frac{\omega_{0I}^4}{\omega_{0\Pi}^2}\right)}{8\sigma_\Pi\tau_\Pi\eta_{\alpha\Pi}(f_{1\Pi} + f_{2\Pi})} \tag{13}$$

where

$$\begin{cases} C_1 = \left(\frac{\omega_{0\Pi}^4}{\omega_{0I}^2} + 3\omega_{0I}^2 + 3\omega_{0\Pi}^2 + \frac{\omega_{0I}^4}{\omega_{0\Pi}^2}\right)^2 \\ C_2 = \frac{\omega_{0\Pi}^8}{\omega_{0I}^4} + \frac{8\omega_{0\Pi}^6}{\omega_{0I}^2} + 16\omega_{0I}^4 + 24\omega_{0\Pi}^4 + 32\omega_{0I}^2\omega_{0\Pi}^2 \\ C_3 = \frac{\omega_{0I}^4}{\omega_{0\Pi}^4} + \frac{\omega_{0\Pi}^2}{\omega_{0I}^2} + \frac{3\omega_{0I}^2}{\omega_{0\Pi}^2} + 3 \end{cases} \tag{14}$$

3. Simulation Analysis

Laser crystal and output mirror are important components in the laser system. Laser crystal parameters (doping concentration and length) and output mirror transmittance greatly influence the threshold pump power and output power, especially in the quasi-three-level system. Next come simulations and analyses of laser crystal parameters and output mirror transmittance related to the threshold pump power, output power, and intracavity power of the 946 nm LG_{01} mode vortex laser and the threshold pump power and output power of the 1030 nm LG_{01} mode vortex laser. The simulation results can provide a reference for subsequent experiments.

The important parameters used in the simulation of the oscillation characteristics of 946 and 1030 nm LG_{01} mode vortex lasers are shown in Table 1. Referring to the previous literature, the doping concentration of the Nd:YAG crystal is set at 1%, and the particle number density of the corresponding ground state energy level is $1.38 \times 10^{17}/mm^3$. The transmittance of the 1030 nm resonator's total reflection mirror to the 946 nm laser is 99%, so the insertion loss is $R_{loss} = 1 - T = 0.01$. The absorption coefficient α_Π of the Yb:YAG crystal to 946 nm laser is set as 0.5 cm^{-1}, and the length of the Yb:YAG crystal is set as 2 mm, so the absorption loss is $\gamma_{\alpha I} = 1 - \exp(-\alpha_\Pi d_\Pi) = 0.095$. When the transmittance of the output mirror is 1%, 3%, 5%, and 10%, the relationship between the threshold pump power, output power, and intracavity power of the 946 nm LG_{01} mode vortex laser and the length of the Nd:YAG crystal are shown in Figure 3a–c, respectively. When the length of the Nd:YAG crystal is 0–10 mm, the threshold pump power initially decreases rapidly, and then the trend of threshold pump power becomes flat after the crystal length is 2 mm; the output power increases rapidly before the crystal length is 3 mm, after which the growth rate slows down and gradually declines. The variation of intracavity power with the increase of crystal length is consistent with that of output power with the increase of crystal length. Combining the threshold pump power and output power, we set the length of the Nd:YAG crystal as 3 mm. When the pump power is 20 W and the length of the Nd:YAG crystal is 3 mm, the relationship between the threshold pump power, output power, and intracavity power of the 946 nm LG_{01} mode vortex laser and the output mirror transmittance are shown in Figure 3d–f. The threshold pump power increases with the increase of the output mirror transmittance, and the intracavity power has the opposite variation. The output power first increases and then decreases with the increase of the output mirror transmittance. The transmittance is 2.5–25%, and the output power exceeds 1 W. On this basis, we set the output mirror transmittance at 946 nm as 2.5%.

Table 1. The important parameters used in the simulation of the oscillation characteristics of the 946 and 1030 nm LG$_{01}$ mode vortex lasers [41–45].

Parameter	Nd:YAG	Yb:YAG
λ_p [nm]	808	946
L_{0I}	0.05	0.05
σ [cm^2]	4×10^{-20}	1.8×10^{-20}
τ [µs]	230	950
α [cm^{-1}]	8 (808 nm)	0.56 (946 nm)
f_1	0.0074	0.046
f_2	0.6	0.7
ω_0 [µm]	200	180
a and b [µm]	200 and 100	-
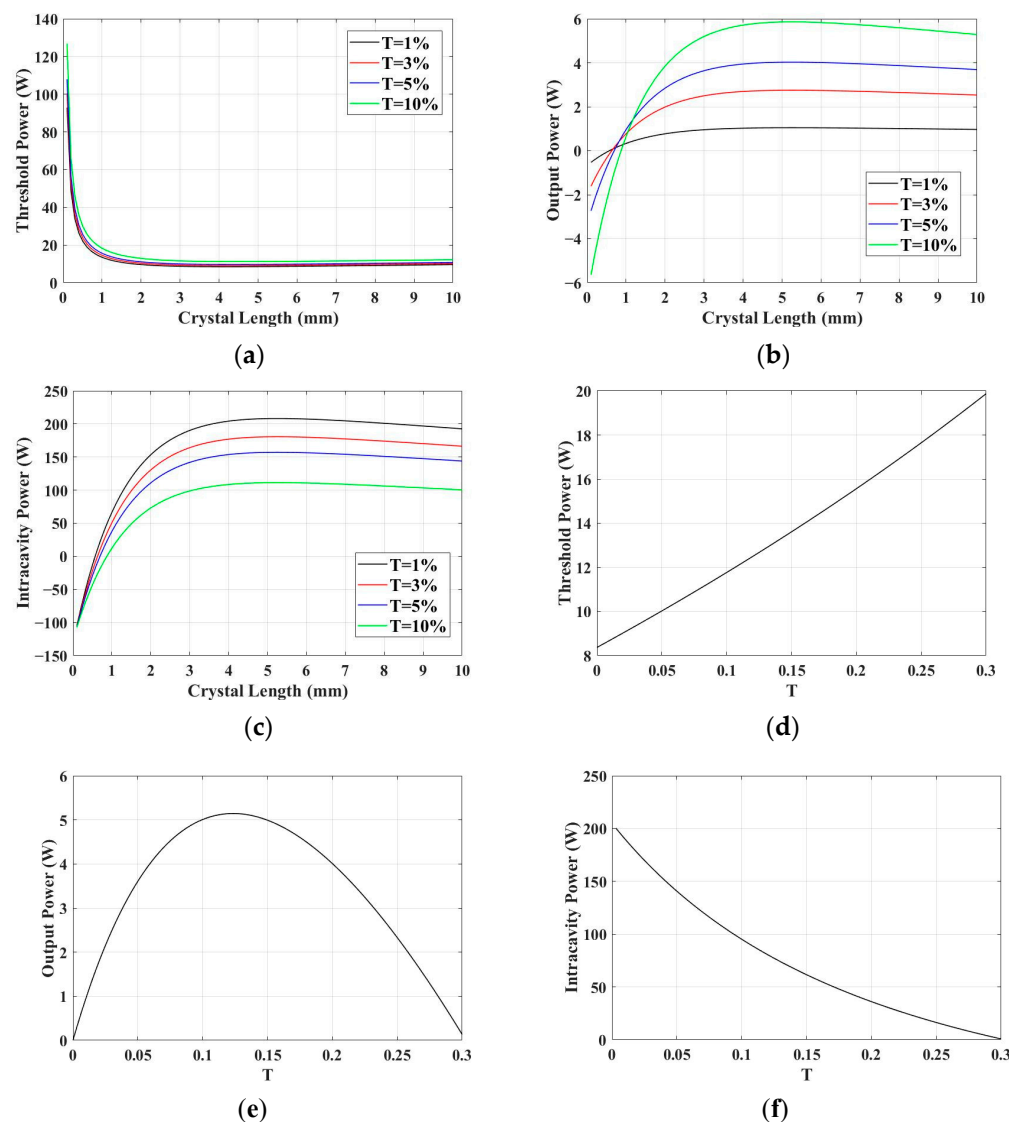
Figure 3. The relationship between (**a**) the threshold pump power, (**b**) output power, and (**c**) intracavity power of the 946 nm LG$_{01}$ mode vortex laser and the length of the Nd:YAG crystal at a pump power of 20 W; the relationship between (**d**) the threshold pump power, (**e**) output power and (**f**) intracavity power of the 946 nm LG$_{01}$ mode vortex laser and the output mirror transmittance at a pump power of 20 W and Nd:YAG crystal length of 3 mm.

Aligned with the study on the doping ion concentration of the Yb:YAG crystal, the doping concentration of Yb^{3+} is set at 0.5%, and the particle number density of the corresponding ground state energy level is $6.9 \times 10^{16}/\text{mm}^3$. When the transmittance of the output mirror is 1%, 3%, 5%, and 10%, the relationship between the threshold pump power and output power of the 1030 nm LG$_{01}$ mode vortex laser and the length of the Yb:YAG crystal are shown in Figure 4a,b, respectively. When the length of the Yb:YAG crystal is 0–10 mm, the threshold pump power originally decreases rapidly, and then the trend of threshold pump power becomes flat after the crystal length is 2 mm; the output power gradually increases as the length of the crystal increases. In addition, considering the intracavity loss of the Yb:YAG crystal to 946 nm laser, the crystal length should not be too long. Therefore, we set the Yb:YAG crystal length as 2 mm. When the pump power is 20 W and the length of Yb:YAG crystal is 2 mm, the relationship between the threshold pump power and output power of the 1030 nm LG$_{01}$ mode vortex laser and the output mirror transmittance are shown in Figure 4c,d. The threshold pump power increases with the increase of the output mirror transmittance. As the output mirror transmittance increases, the output power first increases rapidly, then decreases slowly. The lower operating threshold is preferred, so we set the output mirror transmittance at 1030 nm as 4%.
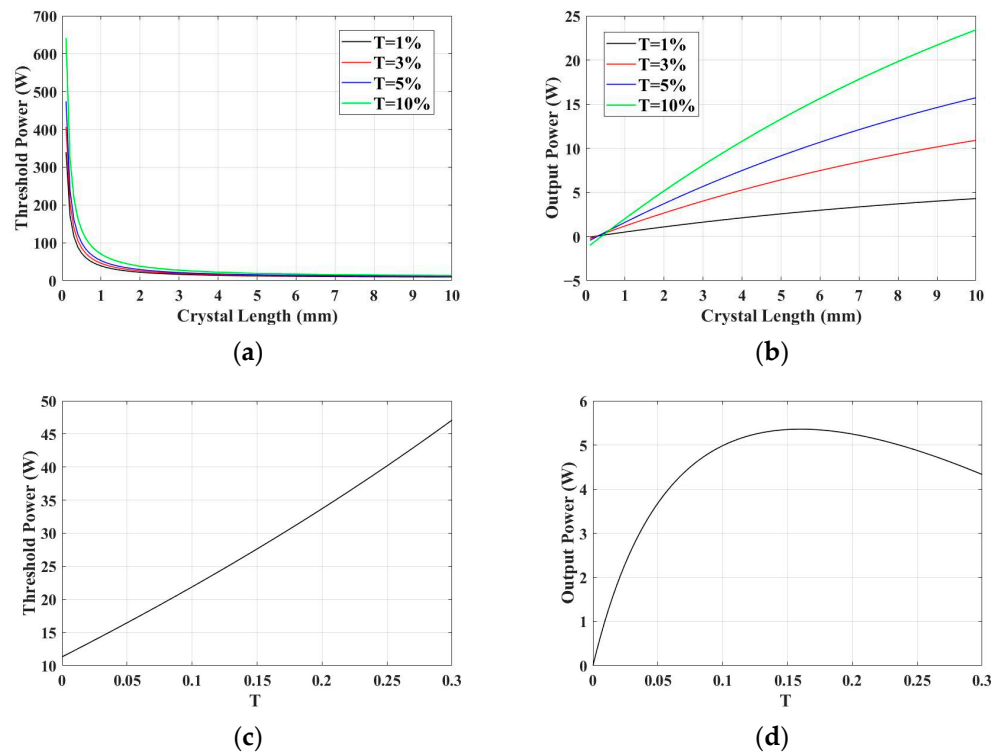
Figure 4. The relationship between (**a**) the threshold pump power and (**b**) the output power of the 1030 nm LG$_{01}$ mode vortex laser and the length of the Yb:YAG crystal at a pump power of 20 W; the relationship between (**c**) the threshold pump power and (**d**) output power of the 1030 nm LG$_{01}$ mode vortex laser and the output mirror transmittance at a pump power of 20 W and Yb:YAG crystal length of 2 mm.

4. Experiment Setup

The experimental setup of the 946/1030 nm dual-wavelength LG$_{01}$ mode laser is shown in Figure 5. The pump source is an 808 nm laser diode connected and output by a fiber pigtail with a core diameter of 200 μm and a numerical aperture of 0.22. First, the pump beam passes through the lens L$_1$ (f = 43 mm) and is collimated into a parallel beam. Then, it is shaped into an annular beam by a reflector M placed at 45°, where the center of the reflector M is an elliptical etched area (the long axis: $5\sqrt{2}$ mm, the short axis: 5 mm). Then, the beam diameter is adjusted by aperture D, and finally, it is converged into the laser

crystal through lens L_2 (f = 80 mm). The efficiency of the coupling system is 58.5%. The gain medium of the 946 nm laser is a Φ4 mm $\times$ 3 mm 1%-doped Nd:YAG crystal, which is coated with 808 and 946 nm antireflection film on the S_1 side and 946 nm antireflection film on the S_2 side. The gain medium of the 1030 nm laser is a Φ4 mm $\times$ 2 mm 0.5%-doped Yb:YAG crystal and its S_1 and S_2 sides are coated with 946 and 1030 nm antireflection coatings. The two crystals are wrapped with indium foil and installed in water-cooled fixtures made of red copper, and the temperature is controlled at 15 °C. The resonator of this laser includes 946 and 1030 nm resonators. The 946 nm resonator is composed of M_1, Nd:YAG crystal and M_2, and its cavity length is 75 mm. The 1030 nm resonator is composed of the M_3, Yb:YAG crystal, and M_2, and its cavity length is 35 mm. M_1 is a plane-concave mirror (curvature radius: 300 mm). Its S_1 and S_2 sides are coated with 808 and 1064 nm antireflection films, and the S_2 side is also coated with 946 nm high-reflection film. M_3 is also a plane-concave mirror (curvature radius: 300 mm). Its S_1 side is coated with a 946 nm antireflection film, and its S_2 side is coated with a 946 nm antireflection film and 1030 nm high-reflection film. M_2 is a plane-plane mirror, and its S_1 and S_2 sides are coated according to the simulation results. The final transmittance of M_2 to 946 and 1030 nm is 2.5% and 3.9%, respectively. The output laser is divided into 946 and 1030 nm LG_{01} mode vortex lasers by dichroic mirror M_4, which is convenient for measuring the parameters of different wavelength lasers separately.
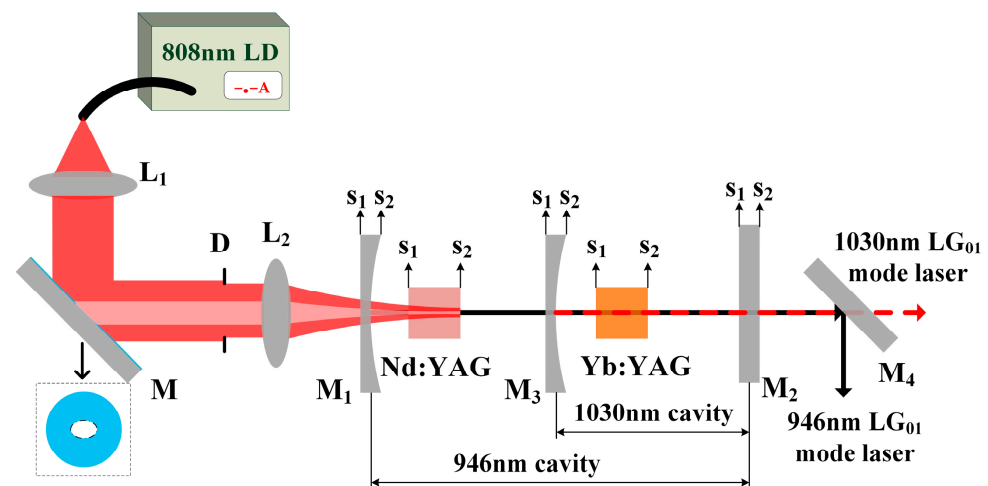
Figure 5. The experimental setup of the 946/1030 nm dual-wavelength LG_{01} mode laser.

5. Results and Discussion

We used the fiber-optic spectrometer (StellarNet, BW-UVN-50) to measure the spectra of the output laser, and the results are shown in Figure 6. Notably, the 808 nm pump laser is not completely absorbed at the high pump power state. We used an RG830 glass filter during the experiment to absorb the residual pump laser. When the pump power of the annular beam is 20 W, the center wavelength of the dual-wavelength laser is 946.48 and 1029.49 nm. The results show that the intracavity cascade pumped scheme successfully achieves the dual-wavelength laser.

Vortex lasers with opposite handedness have the same threshold pump power, so the handedness of vortex lasers directly generated without pre-regulation is easy to change randomly. In order to reduce the insertion loss caused by additional optical elements, a stable handedness of the 946 nm LG_{01} mode vortex laser has been achieved by adjusting the transverse position of the Nd:YAG crystal [39]. A mode converter composed of cylindrical lenses converts the generated vortex laser into a Hermite–Gaussian (HG) laser. The vortex laser's topological charge and handedness change are determined by the number of node lines and the direction of the long axis of the HG laser. The 946 nm vortex laser is adjusted to a direction parallel to the optical axis by a reflector to facilitate the measurement. The measurement diagram and results are shown in Figure 7. By carefully adjusting the lateral

position or pitch angle of the laser crystals, the long-axis of the 946 and 1030 nm HG_{01} mode lasers have the same handedness over the whole pump range. The results show that the 946 and 1030 nm lasers are LG_{01} mode and have the same handedness.
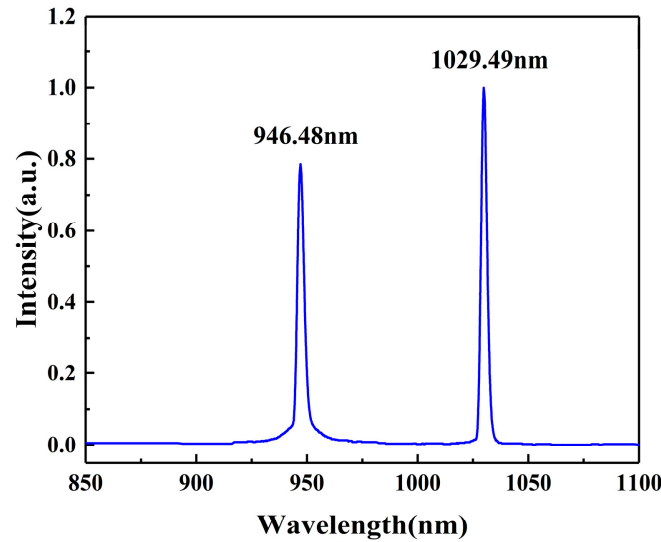

Figure 6. The spectrogram of the dual-wavelength laser.
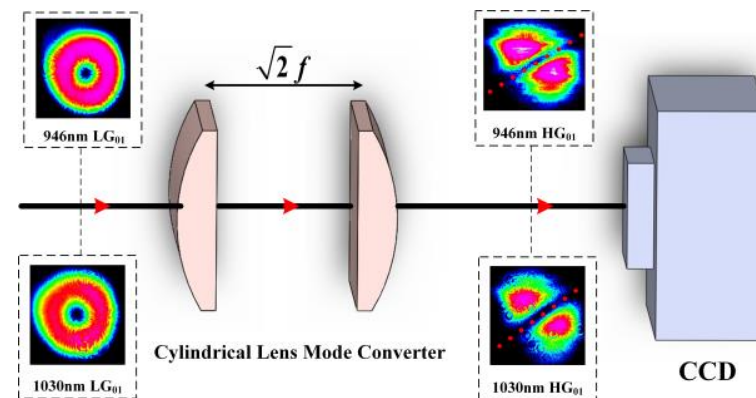
Figure 7. The schematic diagram of the output laser mode and the measurement results.

Further, we carried out experiments and concluded the relationship between the power of the 946 and 1030 nm LG_{01} mode vortex lasers and the pump power of the annular beam, respectively, and the results are shown in Figure 8. When the pump power of the annular beam is 9.7 W, the 946 nm LG_{01} mode vortex laser comes to the start of the output; When the pump power of the annular beam is increased to 11.9 W, the 946 and 1030 nm LG_{01} mode vortex laser start to output simultaneously. When the pump power of the annular beam is increased to 16.1 W, the output power of the 946 and 1030 nm LG_{01} mode vortex laser is consistent, and their size is 0.277 W; When the pump power of the annular beam is 20 W, the output power of 946 and 1030 nm LG_{01} mode vortex lasers is 0.404 and 0.510 W, while the corresponding slope efficiency is 3.6% and 6.2% respectively. The total optical-optical conversion efficiency is 4.6%. Since the full mirror M_3 and Yb:YAG crystal will bring losses to the 946 nm laser oscillation, this is one of the reasons for the lower output power and slope efficiency of the 946 nm LG_{01} mode laser. Another reason is that the dual-wavelength vortex laser is output only in a single handedness, and the laser with opposite handedness is suppressed.
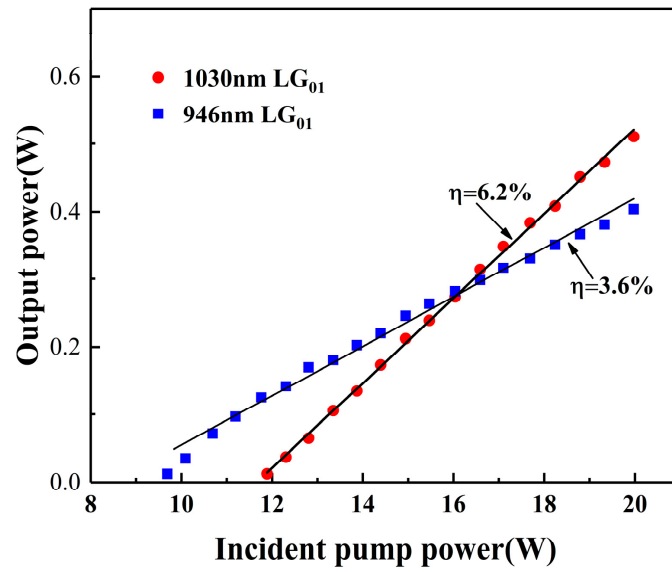
Figure 8. The relationship between the power of the 946/1030 nm LG_{01} mode vortex laser and the pump power of the annular beam.

The output power of the 946/1030 nm LG_{01} mode vortex laser and 808 nm LD varies steadily over time, shown in Figure 9. The output power of the 946 and 1030 nm vortex lasers was recorded every 2 min for a total test time of 1 h. The output power of the 946 and 1030 nm LG_{01} mode lasers fluctuates by 4.02% and 4.23% with the time, respectively. However, the total output power fluctuation is 0.91%, which is smaller than the fluctuation of the 946 and 1030 nm LG_{01} mode vortex lasers, respectively. This phenomenon indicates weak competition between the output power of the dual-wavelength vortex laser. In addition, the pump power of 808 nm LD fluctuates by 0.37% over time.
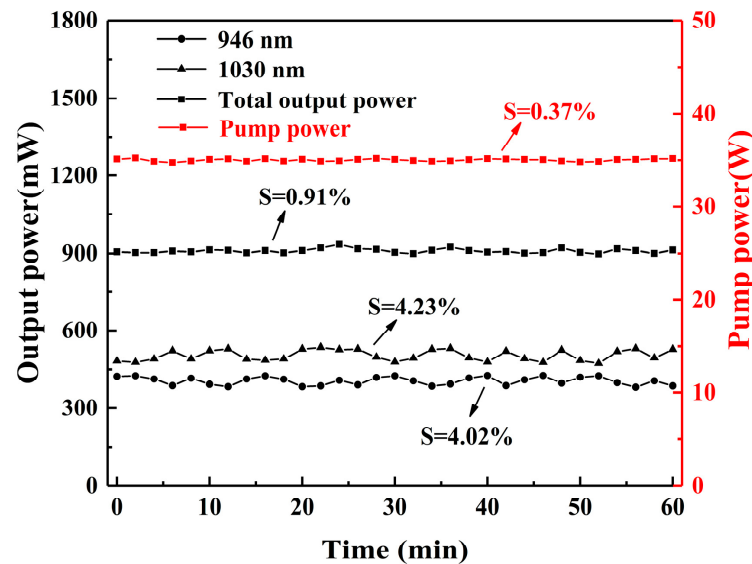
Figure 9. The power stability of the 946/1030 nm LG_{01} mode vortex laser and 808 nm LD with time.

The trend of the beam quality factors M^2 of the 946/1030 nm LG_{01} mode vortex laser with incident pump power as well as time is given in (a) and (b) in Figure 10, respectively. The theoretical value of the beam quality factor M^2 for the LG_{01} mode vortex laser is 2. When the pump power is 13 W to 20 W, the beam quality factor M^2 for the 946 nm LG_{01} mode vortex beam is in the range of 2.20 to 2.32, and the beam quality factor M^2 for the 1030 nm LG_{01} mode vortex beam is in the range of 2.14 to 2.27. The beam quality factors

M^2 of both 946 and 1030 nm LG_{01} mode vortex lasers increase slightly with increasing pump power. The inset in Figure 10a shows the beam factor test results for the 946 nm and 1030 nm LG_{01} mode vortex lasers at a pump power of 20 W, and the results are 2.32 and 2.27, respectively. In addition, we measured the beam quality factor over time for the 946 and 1030 nm LG_{01} mode vortex lasers at a pump power of 20 W. In the early stage, the beam quality factors of the 946 and 1030 nm vortex lasers are relatively stable, and with the increase of time, the beam quality factors of the 946 and 1030 nm vortex lasers show a slowly rising trend due to the accumulation of thermal effects.
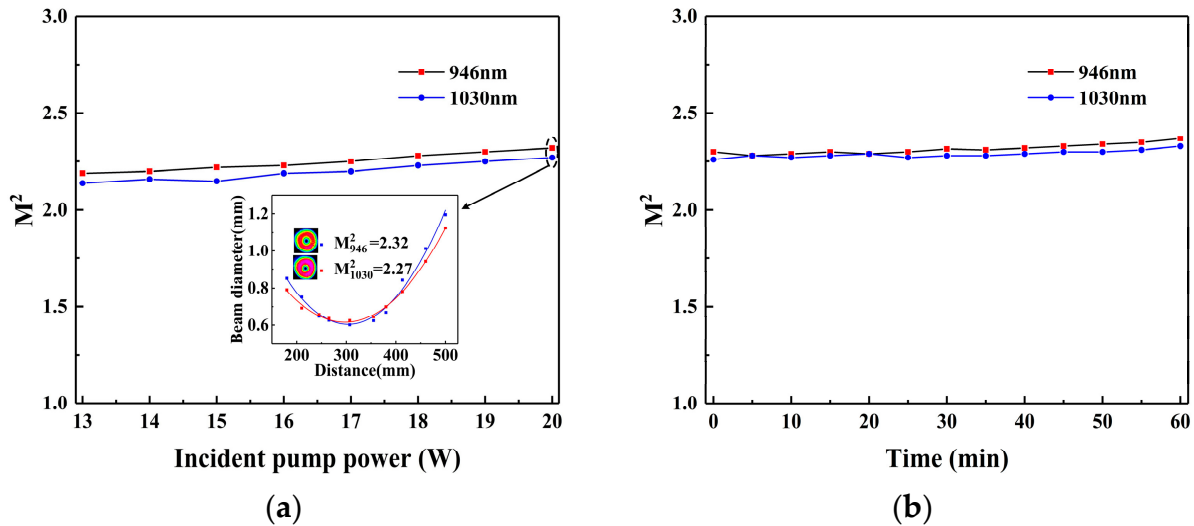
Figure 10. The relationships between the beam quality factors M^2 of the 946/1030 nm LG_{01} mode vortex laser and (**a**) pump power and (**b**) time.

At present, the phase structure of LG-mode laser is mainly measured by the iterative phase retrieval methods and interferometric methods. Using an iterative phase retrieval method, the spiral phase structures of the vortex laser (the tightly focused vortex laser [46], vortex laser containing both a fundamental field and its copropagating second harmonic field [47]) were characterized. Based on the Mach–Zehnder interferometer, the interference of the LG_{01} mode laser with a plane wave or spherical wave was carried out, and the interference pattern with Y-shaped stripes or single-arm spiral stripes proved that the output laser has a wavefront phase $\exp(i\phi)$ [48,49]. In addition, based on the Michelson interferometer, the self-interference of the 4th-order vortex laser was also carried out, and the interference pattern containing a pair of fork-shaped stripes (four forks separated from one singularity) demonstrated that the output laser has the spiral phase $\exp(i4\phi)$ [50]. We also used the self-interference method to measure the wavefront phase of the 946 and 1030 nm LG_{01} mode vortex lasers. The optical path diagram of the measuring device and the results are shown in Figure 11a,b. The output laser is at first divided into two beams of transmitted laser and reflected laser with equal irradiance through the spectroscope G_1, in which the reflected laser passes through the mirror M_1 and then passes through the spectroscope G_1 again. The transmitted laser passes through the compensation plate G_2, the mirror M_2, the compensation plate G_2 and then passes through the spectroscope G_1 again. Finally, the two lasers come to the CCD element and have an interference there. We adjust the front and rear positions of mirror M_1 to make the optical paths of the two paths equal. The self-interference patterns of the 946 and 1030 nm lasers both contain a pair of opposite Y-shaped fringes, which are marked with dashed red lines. Separating a fork from a singularity indicates that the 946/1030 nm LG_{01} mode vortex laser contains the wavefront phase $\exp(i\phi)$.
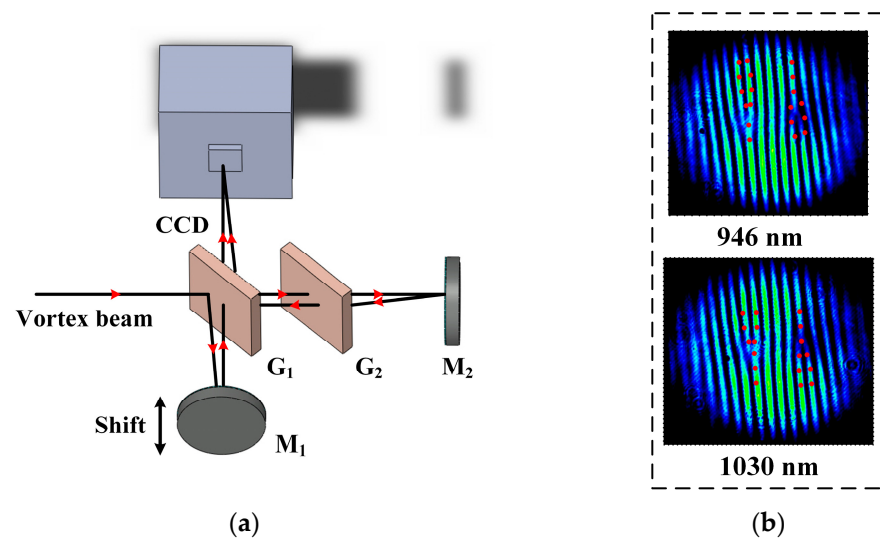
Figure 11. (**a**) The optical path diagram of the wavefront phase detection device, and (**b**) the measurement results.

6. Conclusions

In summary, a novel 946/1030 nm dual-wavelength LG_{01} mode vortex laser is designed and experimentally studied in this paper. Firstly, the theoretical model of oscillation characteristics of intracavity cascade pumped dual-wavelength LG_{01} mode vortex laser considering the reabsorption effect is established, and the length of the laser crystal and the transmittance of the output mirror are simulated and analyzed related to the oscillation characteristics of the 946 and 1030 nm LG01 mode vortex lasers. Finally, the experimental setup is built, and the parameters of the 946 nm and 1030 nm LG_{01} mode lasers are presented, respectively. With the annular-beam pump power of 20 W, the output power is 0.404 and 0.510 W, and the slope efficiency is 3.6% and 6.2% for the 946 and 1030 nm LG_{01} mode vortex lasers. The total optical-optical conversion efficiency is 4.6%. For the maximum output power, the power fluctuates by 4.02% and 4.23% within 1 h. The beam quality factors M^2 are 2.32 and 2.27 for the 946 and 1030 nm LG_{01} mode vortex lasers, respectively. The interference patterns of the 946 and 1030 nm lasers measured by the self-interference method contain a pair of opposite Y-shaped fringes, indicating that the generated dual-wavelength vortex laser has the wavefront phase $\exp(i\phi)$. The 946/1030 nm dual-wavelength LG_{01} mode vortex laser is developed for the first time, and the feasibility of intracavity pumping for dual-wavelength LG_{01} mode vortex laser is verified, which is of great significance for research on dual-wavelength intracavity sum-frequency.

Author Contributions: Conceptualization, Y.Y. and Y.L.; Data curation, Y.Y.; Formal analysis, Y.Y.; Funding acquisition, Y.L. and C.Y.; Investigation, Y.Y.; Methodology, Y.Y.; Project administration, Y.L. and C.Y.; Resources, Y.L.; Software, Y.Y.; Supervision, Y.Y. and Y.L.; Validation, Y.Y., Y.L. and C.W.; Visualization, Y.Y.; Writing–original draft, Y.Y.; Writing–review and editing, Y.Y., Y.L. and C.Y. All authors have read and agreed to the published version of the manuscript.

Institutional Review Board Statement: Not applicable.

Informed Consent Statement: Not applicable.

Data Availability Statement: Not applicable.

Conflicts of Interest: The authors declare that they have no known competing financial interests or personal relationships that could have appeared to influence the work reported in this paper.

References

1. He, W.; Li, D.; Zhu, L.Q.; Dong, M.L.; Luo, F. Tunable multiwavelength erbium-doped fiber laser employing PM-FBG and Mach–Zehnder interferometer with optical fiber delay line. *IEEE Photon. J.* **2017**, *9*, 2695671. [CrossRef]
2. He, W.; Yuan, H.W.; Lou, X.P.; Zhu, L.Q.; Dong, M.L. Multi-wavelength switchable erbium-doped fiber laser based on a hybrid filter incorporating a bi-tapered mach-zehnder interferometer and sagnac loop. *Phys. Scr.* **2019**, *94*, 125502. [CrossRef]
3. Chen, J.J.; Wei, W.Q.; Qin, J.L.; Yang, B.; Huang, J.Z.; Wang, Z.H.; Wang, T.; Yu, C.Y.; Zhang, J.J. Multi-wavelength injection locked semiconductor comb laser. *Photonics Res.* **2022**, *10*, 1840–1847. [CrossRef]
4. Liu, L.; Dai, C.; Wang, X.-Z. A continuous 1052 nm and 1061 nm dual-wavelength Nd:YAG laser. *Optoelectron. Lett.* **2020**, *16*, 181–184. [CrossRef]
5. Jaffres, L.; Labruyère, A.; Couderc, V.; Carreaud, J.; Maître, A.; Boulesteix, R.; Brenier, A.; Boulon, G.; Guyot, Y.; Rabinovitch, Y.; et al. Gain structuration in dual-wavelength Nd: YSAG ceramic lasers. *Opt. Express* **2012**, *20*, 25596–25602. [CrossRef] [PubMed]
6. Akbari, R.; Zhao, H.; Major, A. High-power continuous-wave dual-wavelength operation of a diode-pumped Yb: KGW laser. *Opt. Lett.* **2016**, *41*, 1601–1604. [CrossRef]
7. Wang, B.B.; Gao, C.C.; Dou, R.Q.; Nie, H.K.; Sun, G.H.; Liu, W.P.; Yu, H.J.; Wang, G.J.; Zhang, Q.L.; Lin, X.C.; et al. Dual-wavelength mid-infrared CW and Q-switched laser in diode end-pumped Tm,Ho:GdYTaO$_4$ crystal. *Laser Phys. Lett.* **2018**, *15*, 025801. [CrossRef]
8. Shang, L.H.; Wen, Y.; Li, T.Y.; Guo, Y.Y.; Wang, Y.H.; Wu, C.T.; Wang, C.; Jin, G.Y. Pulse peaks synchronize dual-wavelength laser based on Q-switch delay trigger. *Infrared Phys. Technol.* **2021**, *116*, 103751. [CrossRef]
9. Lin, H.F.; Zhu, W.Z.; Xiong, F.B.; Ruan, J.J. Simultaneous dual-wavelength Q-switched Nd: YAG laser at 1052 and 1073 nm. *Appl. Opt.* **2017**, *56*, 948–951. [CrossRef]
10. Scheller, M.; Baker, C.W.; Koch, S.W.; Moloney, J.V. Dual-Wavelength Passively Mode-Locked Semiconductor Disk Laser. *IEEE Photonics Technol. Lett.* **2016**, *28*, 1325–1327. [CrossRef]
11. Waritanant, T.; Major, A. Dual-wavelength operation of a diode-pumped Nd:YVO$_4$ laser at the 1064.1 & 1073.1 nm and 1064.1 & 1085.3 nm wavelength pairs. *Appl. Phys. B* **2018**, *124*, 87.
12. Qi, Y.Y.; Yu, H.J.; Zhang, J.Y.; Zhang, L.; He, C.J.; Lin, X.C. A compact dual-wavelength Nd:LuVO$_4$ laser with adjustable power-ratio between 1064 nm and 1342 nm lines by controlling polarization dependent loss. *Opt. Commun.* **2017**, *382*, 302–306. [CrossRef]
13. Chen, H.B.; Huang, Y.S.; Li, B.X.; Liao, W.B.; Zhang, G.; Lin, Z.B. Efficient orthogonally polarized dual-wavelength Nd:LaMgB$_5$O$_{10}$ laser. *Opt. Lett.* **2015**, *40*, 4659–4662. [CrossRef]
14. Cheng, H.P.; Liu, Y.C.; Huang, T.L.; Liang, H.C.; Chen, Y.F. Orthogonally polarized single-longitudinal-mode operation in a dual-wavelength monolithic Nd:YAG laser at 1319 nm and 1338 nm. *Photonics Res.* **2018**, *6*, 815–820. [CrossRef]
15. White, A.; Elder, I.; Hall, G. Single longitudinal mode and dual wavelength CW VBG lasers at 1342 nm and 1064 nm. In *Technologies for Optical Countermeasures IX*; SPIE: Bellingham, WA, USA, 2012; Volume 8543, pp. 68–75.
16. Men, S.J.; Liu, Z.J.; Cong, Z.H.; Li, Y.F.; Zhang, X.Y. Electro-optically Q-switched dual-wavelength Nd:YLF laser emitting at 1047 nm and 1053 nm. *Opt. Laser Technol.* **2015**, *68*, 48–51. [CrossRef]
17. Liu, Y.; Dong, Y.; Yu, Y.J.; Wang, C.; Zhang, X.H. Output characteristics of no gain competition 912 nm and 1064 nm dual-wavelength lasers. *Opt. Laser Technol.* **2019**, *115*, 125–128. [CrossRef]
18. Hu, W.W.; Li, Y.L.; Hu, C.W.; Gu, X.K.; Liu, H.X.; Zhang, Y.P.; Zhang, Y.M. Intra-cavity cascaded pumped 912 nm/1030 nm dual-wavelength laser output. *Opt. Commun.* **2019**, *452*, 440–444. [CrossRef]
19. Čižmár, T.; Brzobohatý, O.; Dholakia, K.; Zemánek, P. The holographic optical micro-manipulation system based on counter-propagating beams. *Laser Phys. Lett.* **2011**, *8*, 50–56. [CrossRef]
20. Padgett, M.; Bowman, R. Tweezers with a twist. *Nat. Photonics* **2011**, *5*, 343–348. [CrossRef]
21. Vicidomini, G.; Bianchini, P.; Diaspro, A. STED super-resolved microscopy. *Nat. Methods* **2018**, *15*, 173–182. [CrossRef]
22. Perez-Garcia, B.; Francis, J.; McLaren, M.; Hernandez-Aranda, R.I.; Forbes, A.; Konrad, T. Quantum computation with classical light: The Deutsch Algorithm. *Phys. Lett. A* **2015**, *379*, 1675–1680. [CrossRef]
23. Willner, A.E.; Huang, H.; Yan, Y.; Ren, Y.; Ahmed, N.; Xie, G.; Bao, C.; Li, L.; Cao, Y.; Zhao, Z.; et al. Optical communications using orbital angular momentum beams. *Adv. Opt. Photonics* **2015**, *7*, 66–106. [CrossRef]
24. Wang, B.; Tanksalvala, M.; Zhang, Z.; Esashi, Y.; Jenkins, N.W.; Murnane, M.M.; Kapteyn, H.C.; Liao, C.T. Coherent Fourier scatterometry using orbital angular momentum beams for defect detection. *Opt. Express* **2021**, *29*, 3342–3358. [CrossRef]
25. McCarter, M.R.; Saleheen, A.I.; Singh, A.; Tumbleson, R.; Woods, J.S.; Tremsin, A.S.; Scholl, A.; De Lon, L.E.; Hastings, J.T.; Morley, S.A.; et al. Antiferromagnetic real-space configuration probed by dichroism in scattered x-ray beams with orbital angular momentum. *Phys. Rev. B* **2023**, *107*, L060407. [CrossRef]
26. Li, Z.; Liu, T.; Ren, Y.; Qiu, S.; Wang, C.; Wang, H. Direction-sensitive detection of a spinning object using dual-frequency vortex light. *Opt. Express* **2021**, *29*, 7453–7463. [CrossRef]
27. Wang, B.; Brooks, N.J.; Johnsen, P.C.; Jenkins, N.W.; Esashi, Y.; Binnie, I.; Tanksalvala, M.; Kapteyn, H.C.; Murnane, M.M. High-fidelity ptychographic imaging of highly periodic structures enabled by vortex high harmonic beams. *arXiv* **2023**, arXiv:2301.05563.
28. Gold, M.H. Dual wavelength treatment protocol with a picosecond laser for the reduction of facial wrinkles. *J. Cosmet. Laser Ther.* **2018**, *21*, 147–151. [CrossRef]

29.   Mark Danson, F.; Sasse, F.; Schofield, L.A. Spectral and spatial information from a novel dual-wavelength full-waveform terrestrial laser scanner for forest ecology. *Interface Focus* **2018**, *8*, 20170049. [CrossRef]

30.   Liu, X.Y.; Li, X.W.; Zhao, S.Z.; Yang, K.J.; Guo, L.; Li, T.; Qiao, W.C.; Li, M.; Zhang, B.T.; He, J.L.; et al. Dual-wavelength synchronously mode-locked Tm-doped bulk laser with terahertz frequency beating. *Chin. Opt. Lett.* **2019**, *17*, 091401. [CrossRef]

31.   Kerdoncuff, H.; Christensen, J.B.; Brasil, T.B.; Novikov, V.A.; Polzik, E.S.; Hald, J.; Lassen, M. Cavity-enhanced sum-frequency generation of blue light with near-unity conversion efficiency. *Opt. Express* **2020**, *28*, 3975–3984. [CrossRef]

32.   Hall, D.G.; Smith, R.J.; Rice, R.R. Pump-size effects in Nd: YAG lasers. *Appl. Opt.* **1980**, *19*, 3041–3043. [CrossRef] [PubMed]

33.   Hall, D.G. Optimum mode size criterion for low-gain lasers. *Appl. Opt.* **1981**, *20*, 1579–1583. [CrossRef] [PubMed]

34.   Laabs, H.; Ozygus, B. Excitation of Hermite Gaussian modes in end-pumped solid-state lasers via off-axis pumping. *Opt. Laser Technol.* **1996**, *28*, 213–214. [CrossRef]

35.   Chu, S.C.; Chen, Y.T.; Tsai, K.F.; Otsuka, K. Generation of high-order Hermite-Gaussian modes in end-pumped solid-state lasers for square vortex array laser beam generation. *Opt. Express* **2012**, *20*, 7128–7141. [CrossRef] [PubMed]

36.   Koshel, R.J. Novel methods of intracavity beam shaping. In *Laser Beam Shaping II*; SPIE: Bellingham, WA, USA, 2001; Volume 4443, pp. 47–57.

37.   Zhao, Y.G.; Liu, Q.Y.; Zhou, W.; Shen, D.Y. ~1 mJ pulsed vortex laser at 1645 nm with well-defined helicity. *Opt. Express* **2016**, *24*, 15596–15602. [CrossRef] [PubMed]

38.   Liu, Q.Y.; Zhao, Y.G.; Ding, M.M.; Yao, W.C.; Fan, X.L.; Shen, D.Y. Wavelength-and OAM-tunable vortex laser with a reflective volume Bragg grating. *Opt. Express* **2017**, *25*, 23312–23319. [CrossRef]

39.   Yang, Y.S.; Li, Y.L.; Wang, C.; Yang, C. Research on 946 nm LG_{01} mode laser considering thermal effect. *Laser Phys.* **2022**, *32*, 095801. [CrossRef]

40.   Kim, J.W.; Clarkson, W.A. Selective generation of Laguerre–Gaussian (LG_{0n}) mode output in a diode-laser pumped Nd:YAG laser. *Opt. Commun.* **2013**, *296*, 109–112. [CrossRef]

41.   Hanson, F. Efficient operation of a room-temperature Nd:YAG 946-nm laser pumped with multiple diode arrays. *Opt. Lett.* **1995**, *20*, 148–150. [CrossRef]

42.   Clarkson, W.; Koch, R.; Hanna, D. Room-temperature diode-bar-pumped Nd:YAG laser at 946 nm. *Opt. Lett.* **1996**, *21*, 737–739. [CrossRef]

43.   Lindsay, I.D.; Ebrahimzadeh, M. Efficient continuous-wave and Q-switched operation of a 946-nm Nd:YAG laser pumped by an injection-locked broad-area diode laser. *Appl. Opt.* **1998**, *37*, 3961–3970. [CrossRef]

44.   Fan, T.; Byer, R. Modeling and CW operation of a quasi-three-level 946 nm Nd:YAG laser. *IEEE J. Quantum Electron.* **1987**, *23*, 605–612.

45.   Wang, X.D.; Zhao, Z.W.; Zeng, X.H.; Mao, H.M.; Liang, X.Y. Study on Spectra and Laser Properties of 0.5at% Yb:YAG Crystal. *J. Synth. Cryst.* **2014**, *43*, 758–764.

46.   Saito, T.; Takeo, Y.; Mimura, H. Precise characterization of focused vortex beams. *Jpn. J. Appl. Phys.* **2017**, *56*, 092501. [CrossRef]

47.   Esashi, Y.; Liao, C.-T.; Wang, B.; Brooks, N.; Dorney, K.M.; Hernández-García, C.; Kapteyn, H.; Adams, D.; Murnane, M. Ptychographic amplitude and phase reconstruction of bichromatic vortex beams. *Opt. Express* **2018**, *26*, 34007–34015. [CrossRef]

48.   Liu, Q.Y.; Zhao, Y.G.; Zhou, W.; Shen, D.Y. Vortex operation in Er:LuYAG crystal laser at 1.6 μm. *Opt. Mater.* **2017**, *71*, 31–34. [CrossRef]

49.   He, H.S.; Chen, Z.; Dong, J. Direct generation of vector vortex beams with switchable radial and azimuthal polarizations in a monolithic Nd:YAG microchip laser. *Appl. Phys. Express* **2017**, *10*, 052701. [CrossRef]

50.   Qiao, Z.; Xie, G.Q.; Wu, Y.H.; Yuan, P.; Ma, J.G.; Qian, L.J.; Fan, D.Y. Generating High-Charge Optical Vortices Directly from Laser Up to 288th Order. *Laser Photonics Rev.* **2018**, *12*, 1800019. [CrossRef]